Mediterranean Marine Science

Vol 15, No 4 (2014)

Vol 15, No 4 (2014) special issue

A high-resolution hydrodynamic-biogeochemical coupled model of the Gulf of Cadiz – Alboran Sea region.

D. M. MACIAS, C. T. GUERREIRO, L. PRIETO, A. PELIZ, J. RUIZ

doi: 10.12681/mms.841

Research Article

Mediterranean Marine Science
Indexed in WoS (Web of Science, ISI Thomson) and SCOPUS
The journal is available on line at http://www.medit-mar-sc.net
DOI: http://dx.doi.org/10.12681/mms.841

A high-resolution hydrodynamic-biogeochemical coupled model of the Gulf of Cadiz – Alboran Sea region

D. MACIAS[1], C.T. GUERREIRO[2,3], L. PRIETO[2], A. PELIZ[3] and J. RUIZ[2]

[1] European Commission. Joint Research Center. Institute for Environment and Sustainability
Via E. Fermi, 21047. 21020-Ispra, Varese, Italy
[2] Spanish Council for Scientific Research. Instituto de Ciencias Marinas de Andalucía. Avd.
Republica Saharaui, s/n. 11510- Pto Real, Cadiz, Spain
[3] Instituto Dom Luíz, Faculdade de Ciências da Universidade de Lisboa, Campo Grande, Lisboa Portugal

Corresponding author: diego.macias-moy@jrc.ec.europa.eu

Handling Editor: Ioanna Siokou

Received: 20 March 2014; Accepted: 22 September 2014 ; Published on line: 22 December 2014

Abstract

The southern Iberia regional seas comprise the Gulf of Cadiz and the Alboran Sea sub-basins connected by the narrow Strait of Gibraltar. Both basins are very different in their hydrological and biological characteristics but are, also, tightly connected to each other. Integrative studies of the whole regional oceanic system are scarce and difficult to perform due to the relative large area to cover and the different relevant time-scales of the main forcing in each sub-basin. Here we propose, for the first time, a fully coupled, 3D, hydrodynamic-biogeochemical model that covers, in a single domain (~2km resolution) both marine basins for a 20-year simulation (1989-2008). Model performance is assessed against available data in terms of spatial and temporal distribution of biological variables. In general, the proposed model is able to represent the climatological distribution of primary and secondary producers and also the main seasonality of primary production in the various sub-regions of the analyzed basins. Potential causes of the observed mismatches between model and data are identified and some solutions are proposed for future model development. We conclude that most of these mismatches could be attributed to the missing tidal forcing in the actual model configuration. This model is a first step towards obtaining a meaningful tool to study past and future oceanographic conditions in this important marine region, which constitutes the unique connection between the Mediterranean Sea and the open ocean.

Keywords: Numerical modelling, Tidal effect, Surface Chlorophyll, Gulf of Cadiz, Alboran Sea, Strait of Gibraltar.

Introduction

The southern Iberia marginal seas are a complicated oceanographic area due to the presence of two marine basins with particularly different characteristics, the Atlantic Ocean and the Mediterranean Sea. Both basins are connected by a constricted connection known as the Strait of Gibraltar which is only 14 km wide at its narrowest section. At both sides of the Strait, there are two substantially different regional sub-basins, the Gulf of Cadiz (GoC) on the Atlantic side and the Alboran Sea in the Mediterranean part.

The GoC is a mesotidal basin with a wide continental shelf and some important rivers discharging in its coastal zone. The GoC presents medium primary productivity levels (e.g. Echevarria *et al*., 2009) mainly associated to the coastal zone, to frontal regions and to the discharges of the main river, the Guadalquivir (Navarro & Ruiz, 2006; Garcia-Lafuente & Ruiz, 2007; Prieto *et al*., 2009). All this primary productivity is channelled up through the food web to maintain quite high fish productivity and diversity (Catalan *et al*., 2006; Ruiz *et al*., 2009) that sustain an economically important fishing activity in the region (Baldó *et al*., 2006).

On the other side, in the Alboran Sea, there are no important river discharges, the tidal influence is much lower, the continental shelf is narrower and one of the main drivers of primary productivity in the region is the inflow of Atlantic waters through the Strait of Gibraltar (Macias *et al*., 2007a). Productivity levels are usually lower than in the GoC (*e.g*. Echevarria *et al*., 2009) while fishery yields are also less important than on the Atlantic side.

Water exchange through the Strait of Gibraltar is due to typically anti-estuarine circulation, with surface Atlantic waters (the Atlantic Jet, AJ) flowing into the Alboran Sea and an outflow of Mediterranean waters in the layer below (*e.g.* Armi & Farmer, 1985). The biogeochemical composition of the AJ is dependent on several aspects such as the original characteristics in the GoC (Navarro *et al.*, 2006), interfacial mixing along the channel of the Strait (*e.g.* Macias *et al.,* 2006; 2007b), and coastal-channel interactions (lateral cross-shelf mixing) driven by tidal motion within the Strait (*e.g.* Vazquez *et al*., 2009; Navarro *et al.,* 2011; Bruno *et*

al., 2013). Any changes in AJ characteristics have a large influence on the dynamics and productivity of the pelagic ecosystem of the Alboran Sea (*e.g.* Ruiz *et al.,* 2001; Macias *et al.,* 2009; Oguz *et al*., 2013).

It is then clear that the dynamics of both sub-basins cannot be fully understood if studied separately and that an integrative approach is much needed in this region. However, integrated field studies (*e.g.* Rubin *et al.,* 1997; Echevarria *et al*., 2009) are difficult to perform due to the different time-scales of forcing mechanisms in the two regions and to the relative large area to cover. Henceforth, locally-focused studies centred either in the GoC (e.g. Navarro *et al*., 2006; Prieto *et al*., 2009), the Alboran Sea (*e.g*. Sarhan *et al*., 2000; Macias *et al*., 2008a, 2009) or the Strait of Gibraltar (*e.g.* Macias *et al*., 2008b; Bruno *et al*., 2013; Ramirez-Romero *et al*., 2014) are much more common.

A numerical model encompassing the marine environment at both sides of the Strait could be an alternative and a very useful tool to quantify the integrated effects and connections within this system. However, and given the heterogeneity of the characteristics of these two interconnected basins it is quite challenging to create a single numerical modelling framework that is able to represent both systems correctly, with a high resolution and covering a multi-year time span. This was accomplished recently by the hydrodynamic model developed in Peliz *et al*. (2013a), where successful multiannual runs for the two basins were presented.

In this manuscript we advance the simulations of Peliz *et al*. (2013a) by coupling a newly developed biogeochemical model specifically tailored to represent the pelagic ecosystem of the GoC and the Alboran Sea.

Material and Methods

We use the *Regional Ocean Modelling System* (ROMS) (*e.g.* Shchepetkin & McWilliams, 2005) coupled with a biological module that describes pelagic aspects of nitrogen cycling. The physical model configuration is extensively explained in Peliz *et al*. (2013a, b) and covers the GoC and Alboran basins (Fig. 1). The model has 32 sigma vertical levels, with moderate stretching at surface, and ~2 x 2 km horizontal resolution. It includes a Mediterranean mass balance that enables correct representation of the exchange through the Strait of Gibraltar. Tidal dynamics are not included in model configuration.

Our biogeochemical simulation covers the period from 1989 to 2008 and outputs are stored in 2-day averages.

Biogeochemical Model: $N_2P_2Z_2D_2$

This model was adapted from the biological code in the ROMS package (based on Fasham *et al*., 1990) following the philosophy of Koné *et al*. (2005) in adopting a double compartment version of the nitrogen-based model (summing eight state variables). The dissolved inorganic nitrogen is represented by nitrate (NO_3) and ammonium (NH_4). Phytoplankton, zooplankton and detritus communities are represented by small (P_s, Z_s and D_s) and large (P_l, Z_l and D_l) groups organisms. Phytoplankton cells are split into nanoplankton (small) and microplankton (large) while zooplankton compartments represent microzooplankton (small) and mesozooplankton (large). A conceptual diagram of the formulated model is shown in Figure 2.

Since our model follows the Fasham *et al*. (1990) model's basic structure, we will mainly focus on our modifications to the code in the following description. The equation parameters are defined in Table 1. Concerning the structure of the model, μ denotes a mortality or breakdown term, ξ an excretion term, and g a grazing term. All state variables are expressed in nitrogen currency (mMol N m^{-3}).

Temporal variations of small and large phytoplankton biomass are governed by biological source-minus-sink terms of the form,

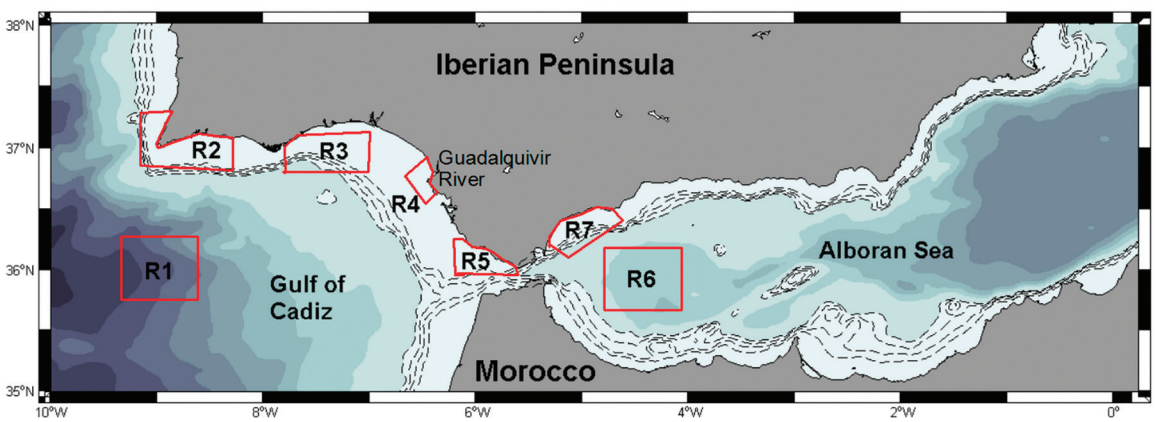

Fig. 1: Modelled domain with main isobaths (each 100 meters) indicated as dashed lines. The seven eco-regions where seasonality of the model is assessed against measured data are indicated by red boxes (see text for explanation). R1 (Open Gulf of Cadiz), R2 (Cape San Vicente), R3 (Cape Santa Maria), R4 (Guadalquivir coastal zone), R5 (Cape Trafalgar), R6 (Western Alboran Gyre) and R7 (Estepona upwelling).

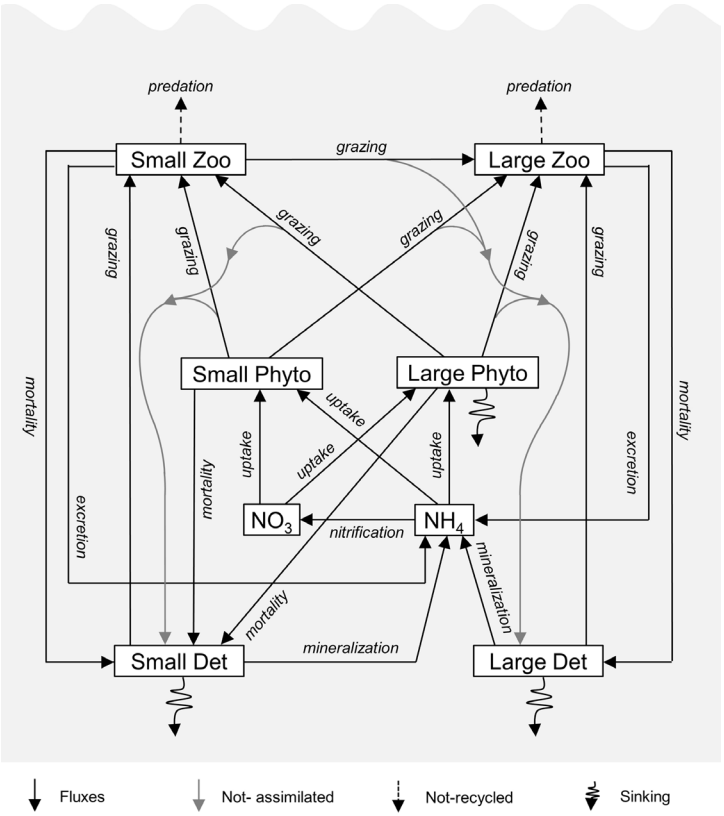

Fig. 2: Conceptual diagram of the biogeochemical model used. Boxes represent state variables and arrows are energy and mass fluxes.

$$sms(P_s)=J_sQ_s(\mathrm{NO}_3)[P_s]+ J_sQ_s(\mathrm{NH}_4)[\mathrm{P_s}]-g_{z_s,P_s}[P_s]-g_{z_l,P_s}[P_s]-\mu_{P_s,D_s}[P_s]\ \text{(I)}$$

$$sms(P_l)=J_lQ_l(\mathrm{NO}_3)[P_l]+ J_lQ_l(\mathrm{NH}_4)[\mathrm{P_l}]-g_{z_s,P_l}[P_l]-g_{z_l,P_l}[P_l]-\mu_{P_l,D_s}[P_l]-L_{P_l}\frac{\partial [P_l]}{\partial z}\quad \text{(II)}$$

Phytoplankton growth rate depends on light and temperature, expressed in the equation by J_i (i stands for small or large), and on nutrient uptake, expressed by $Q_i(NO_3)$ and $Q_i(NH_4)$.

$$J_i=\frac{V_{P_i}PAR\alpha_i}{\sqrt{V_{P_i}^2+PAR^2\alpha_i^2}} \quad (1)$$

$$V_{P_i}=\alpha_i\times 1.066^T \quad (2)$$

$$PAR=PAR_0\exp[-0.5(k_w+k_{Chl}[P_t(k)])\Delta z(k)] \quad (3)$$

The J_i function is controlled by temperature-saturated growth (V_{P_i})(Eppley, 1972), Photosynthetically Available Radiation (PAR), and by initial slope of the P-I curve(α_i). PAR is given by the exponential decay in depth of PAR at surface (PAR_0), where k_w and k_{Chl} are light attenuation due to sea water and chlorophyll, Δz the depth step and $[P_t(k)]$the total phytoplankton concentration at k level.

$$Q_i(NO_3)=\frac{[NO_3]}{K_{i,NH3}+[NO_3]}\ \frac{K_{i,NH4}}{K_{i,NH4}+[NH_4]} \quad (4)$$

$$Q_i(NH_4)=\frac{[NH_4]}{K_{i,NH4}+[NH_4]} \quad (5)$$

Nitrogen limitation is given by a Michaelis-Menten function for nitrate (4) and ammonium (5) where nitrate uptake is assumed to be inhibited in the presence of ammonium, following Parker (1993).$K_{i,NO3}$ and $K_{i,NH4}$ are the half saturation constants for NO_3 and NH_4 uptake, respectively.

The rate of zooplankton grazing $g_{y,x}$, depends on the predator y (small or large zooplankton), the prey x (phytoplankton, detritus or small zooplankton) and maximum grazing rate $g_{\max y}$, food preference $e_{y,x}$, half-saturation constant for ingestion $K_{Z,y}$ and total food available F_{t_y} or each predator,

$$g_{y,x}=g_{\max_y}e_{y,x}\frac{[x]}{K_{Z_y}+F_{t_y}} \quad (6)$$

Small zooplankton consumes preferentially small phytoplankton ($e_{Z_s,\ P_s}$ = 0.7) and less efficiently large phytoplankton and small detritus (e_{Z_s,P_l} = 0.4;e_{Z_s,P_l}=0.3). Large zooplankton grazes preferentially on large phytoplankton (e_{Z_l,P_l} = 0.7), and less efficiently on small phytoplankton, small zooplankton and large detritus (e_{Z_l,P_l} = 0.2;e_{Z_l,Z_s}=0.4; e_{Z_l,D_l}= 0.3).

The remaining phytoplankton loss terms are mortality, represented by a linear rate μ, and vertical sinking only

Table 1. Definition of biogeochemical $N_2P_2Z_2D_2$ model parameters. Where not specifically indicated, they come from the values defined in Koné *et al.* (2005).

Parameter	Definition	Value	Units
k_w	Light attenuation due to seawater	0.06	m^{-1}
k_{Chl}	Light attenuation due to chlorophyll	0.03	$(m^2mgChla)^{-1}$
$r_{C/N,P}$	C/N ratio for phytoplankton	6.625[a]	mMol C $(mMol N)^{-1}$
α_s	Small phytoplankton initial slope of the P-I curve	0.21	$m^{-2}W^{-1}$
α_t	Large phytoplankton initial slope of the P-I curve	0.25	$m^{-2}W^{-1}$
θ	Maximum cellular Chl/Carbon ratio for phytoplankton	0.02	mg Chla $(mg C)^{-1}$
K_s,NO_3	Half-saturation for small phytoplankton NO_3 uptake	0.3	mMol N m^{-3}
K_t,NO_3	Half-saturation for large phytoplankton NO_3 uptake	0.6	mMol N m^{-3}
K_s,NH_4	Half-saturation for small phytoplankton NH_4 uptake	0.2	mMol N m^{-3}
K_t,NH_4	Half-saturation for large phytoplankton NH_4 uptake	0.4	mMol N m^{-3}
K_{PAR}	Half-saturation constant for nitrification	10	W m^{-2}
K_{Zs}	Small zooplankton half-saturation constant for ingestion	0.5	mMol N m^{-3}
K_{Zt}	Large zooplankton half-saturation constant for ingestion	0.8	mMol N m^{-31}
$K_{Zs,P}$	Half-saturation constant of higher predation on small zooplankton	0.05[b]	mMol N m^{-3}
$K_{Zt,P}$	Half-saturation constant of higher predation on large zooplankton	0.005[b]	mMol N m^{-3}
K_D	Half-saturation for detritus sinking	0.5	mMol N m^{-3}
β_s	Small zooplankton assimilation efficiency of food	0.8	n.d.
β_t	Large zooplankton assimilation efficiency of food	0.7	n.d.
$g_{\max_S}$	Maximum small zooplankton grazing rate	1[c]	d^{-1}
$g_{\max_t}$	Maximum large zooplankton grazing rate	0.6	d^{-1}
$e_{Zs,Ps}$	Small zooplankton preference for small phytoplankton	0.7	n.d.
$e_{Zs,Pt}$	Small zooplankton preference for large phytoplankton	0.4	n.d.
$e_{Zs,Ds}$	Small zooplankton preference for small detritus	0.3	n.d.
$e_{Zt,Ps}$	Large zooplankton preference for small phytoplankton	0.2	n.d.
$e_{Zt,Pt}$	Large zooplankton preference for large phytoplankton	0.7	n.d.
$e_{Zt,Zs}$	Large zooplankton preference for small zooplankton	0.4	n.d.
$e_{Zt,Dt}$	Large zooplankton preference for large detritus	0.3	n.d.
ξz_{sA}	Small zooplankton specific excretion rate	0.1	d^{-1}
ξz_{tA}	Large zooplankton specific excretion rate	0.05	d^{-1}
μ_{AN}	Maximum nitrification of NH_4 to NO_3	0.1	d^{-1}
μ_{DsA}	Small detrital breakdown to NH_4 rate	0.1	d^{-1}
μ_{DtA}	Large detrital recycling to NH_4 rate	0.05	d^{-1}
$\mu_{Ps,Ds}$	Small phytoplankton mortality rate to small detritus	0.06[c]	d^{-1}
$\mu_{Pt,Ds}$	Large phytoplankton mortality rate to small detritus	0.04[c]	d^{-1}
$\mu_{Zs,Ds}$	Small zooplankton mortality rate to small detritus	0.08	d^{-1}
$\mu_{Zt,Dt}$	Large zooplankton mortality rate to large detritus	0.04	d^{-1}
$f_{Zs,D}$	Constant rate for predation function of higher predators on small zooplankton	0.1[b]	$(mMol N)^{-1}$ m^3d^{-1}
$f_{Zt,D}$	Constant rate for predation function of higher predators on large zooplankton	0.3[b]	$(mMol N)^{-1}$ m^3d^{-1}
L_{Pt}	Large phytoplankton sinking velocity	2.0[c]	m d^{-1}
L_{Ds}	Small detritus maximum sinking velocity	0.8[c]	m d^{-1}
L_{Dt}	Large detritus maximum sinking velocity	8.0[c]	m d^{-1}

(a) Redfield C/N ratio (106/16), (b) Martin *et al*. (2001) and (c) Oguz *et al*. (2013).

for large phytoplankton, with constant velocity L_{P_i}. Sinking terms were considered for large phytoplankton and detritus since dead particulate tend to sink in the water column, and some species of larger phytoplankton may also sink at slower rate or aggregate with the detritus pool, which may affect phytoplankton dynamics. The algorithm for vertical sinking is based on the Colella & Woodward (1984) piecewise parabolic method and applied at the end of the biological exchanges and reactions.

Changes in zooplankton are controlled by grazing, excretion, mortality and predation terms,

$$sms(Z_s) = g_{Z_s,P_s}[P_s]\beta_s + g_{Z_s,P_i}[P_i]\beta_s + g_{Z_s,D_s}[D_s]\beta_s - g_{Z_i}, {}_{Z_s}[Z_s] - \xi_{Z_sA}[Z_s] - \mu_{Z_s,D_s}[Z_s]F_{Z_s,H}[Z_s]^2 \quad \text{(III)}$$

$$sms(Z_i) = g_{Z_i,P_s}[P_s]\beta_i + g_{Z_i,P_i}[P_i]\beta_i + g_{Z_i,Z_s}[Z_s]\beta_i - g_{Z_i,\,D_i}[D_i]$$
$$\beta_i - \xi_{Z_iA}[Z_i] - \mu_{Z_i,D_i}[Z_i]F_{Z_i,H}[Z_i]^2 \quad \text{(IV)}$$

Zooplankton grazing terms assume that zooplankton assimilates ingested food with β, efficiency while the remaining is transferred to small and large detritus, respectively. The last terms in quadratic form represent zooplankton predation by higher trophic levels (i.e. fish) and do not re-enter the system, being completely lost. Oguz *et al*. (2013) propose the use of a predation function, dependent on zooplankton concentration, instead of a constant rate, enabling relatively strong predation for productive regions and weak for less productive. The implemented predation function $F_{Z_i,H}$ is of the form:

$$F_{Z_i,P} = f_{Z_i,P}\frac{[Z_i]}{K_{Z_i,H} + [Z_i]}$$

Changes in detritus are governed by the following equations:

$$sms(D_s) = g_{Z_s,P_s}[P_s](1-\beta_s) + g_{Z_s,P_i}[P_i](1-\beta_s) + g_{Z_s,D_s}[D_s](-\beta_s)$$
$$+\mu_{P_s,D_s}[P_s] + \mu_{P_i,D_s}[P_i] + \mu_{Z_s,D_s}[Z_s] - \mu_{D_sA}[D_s] - L_{D_s}\frac{\partial[D_s]}{\partial z} \quad \text{(V)}$$

$$sms(D_i) = g_{Z_i,P_s}[P_s](1-\beta_i) + g_{Z_i,P_i}[P_i](1-\beta_i) + g_{Z_i,Z_s}[Z_s](1-\beta_i)$$
$$+g_{Z_i,\,D_i}[D_i](-\beta_i) + \mu_{Z_i,D_i}[Z_i] + \mu_{D_i\mathrm{A}}[D_i] - L_{D_i}\frac{\partial[D_i]}{\partial z} \quad \text{(VI)}$$

The last term expresses detritus sinking, where sinking is stronger in the presence of higher concentrations of detritus that tend to aggregate.

$$L_{D_i,P} = w_{\mathrm{D}_i}\frac{[D_i]}{K_D + [D_i]} \quad (9)$$

Nutrients recycling and uptake processes are given by:

$$sms(NO_3) = -J_sQ_s(NO_3)[P_s] - J_iQ_i(NO_3)[P_i] + \mu_{AN}[NH_4] \quad \text{(VII)}$$

$$sms(NH_4) = -J_sQ_s(NH_4)[P_s] - J_sQ_i(NH_4)[P_i] - \mu_{AN}[NH_4]$$
$$+\xi_{Z_s}A[Z_s] + \xi_{Z_i}A[Z_i] + \mu_{D_sA}[D_s] + \mu_{D_iA}[D_i] \quad \text{(VIII)}$$

Nitrification of NH_4 to NO_3 is done at a constant rate of μ_{AN}. Excretion of zooplankton and detritus recycling, respectively with constant rates of ξ_{Z_iA} and μ_{D_iA}, provide the supply for recycled ammonium.

The bacterial component originally present in the Fasham *et al.* (1995) model has been substituted by detritus recycling parameterization (with constant rates μ_{D_sA} and μ_{D_iA}) following a common approach for coastal settings (*e.g.* Koné *et al.,* 2005; Oguz *et al.,* 2013). This is but a rough approximation that could create problems in some specific areas but also reduce the number of parameters included in the model for which specific information for this particular region is still lacking.

Biogeochemical – hydrodynamic model coupling

The evolution of the biological variables within the previous routine are incorporated in the physical model by adding the source-minus-sink term in the advection-diffusion equation,

$$\frac{\partial B_v}{\partial t} + \mathrm{u}\frac{\partial B_v}{\partial x} + \mathrm{v}\frac{\partial B_v}{\partial y} + \mathrm{w}\frac{\partial B_v}{\partial z} = \frac{\partial}{\partial x}\left(k_x\frac{\partial B_v}{\partial x}\right)$$
$$+\frac{\partial}{\partial y}\left(k_y\frac{\partial B_v}{\partial y}\right) + \frac{\partial}{\partial z}\left(k_z\frac{\partial B_v}{\partial z}\right) + sms\,(B_v) \quad (10)$$

where B_v is the concentration of the biological state variable v. The first term on the left-hand side accounts for tendency and the latter for advection, u and v stand for horizontal water velocity and w for vertical water velocity. On the right side, the first three terms represent horizontal and vertical diffusion, with k_x, k_y, k_z being the respective eddy diffusion coefficients.

In contrast to the null explicit diffusion given to the physical variables in Peliz *et al*. (2013a), due to the dispersive properties of the advection equation, biological state variables needed an explicit diffusion term to avoid numerical problems related with the advection schemes. A 60 m^2s^{-1} horizontal diffusion coefficient was implemented to biological tracers to avoid negative false values.

A third-order upstream-biased accurate predictor–corrector –leapfrog/Adams–Moulton – time step algorithm (Shchepetkin & McWilliams, 2005) is used for tracers. Further numerical options and parameterizations implemented to solve the latter equation (10) are referred in Peliz *et al*. (2013a).

For each time step, the evolution of any biological variable is performed by the advection-diffusion equation, while biological dynamics are computed afterwards in the biological routine. For each baroclinic time step, δt (200 s) the biogeochemical routine is integrated three times, δt/3 ~66.7 s.

Initial and Boundary Conditions. Atmospheric forcing

The initial and open boundary fields for nitrate, phytoplankton and zooplankton were taken from MEDATLAS (http://www.ifremer.fr/medar/) for the Mediterranean and from WOA2005 (www.nodc.noaa.gov/OC5/WOA05) for the Atlantic.

Ammonium initial and boundary fields (not available from the datasets) were obtained by assuming that *[NH4]=[NO3]/2.6*. This ratio was calculated using the information from a dataset of more than 1500 nutrient analyses in the Gulf of Cadiz and Alboran regions (Navarro *et al*., 2006; Prieto *et al.,* 2009).

For the two different phytoplankton functional types, information was gathered from the study regions (Prieto *et a*l., 2009 and unpublished data) and also from the North Atlantic (Huete-Ortega *et al*., 2011), representing open sea regions. As previously described (Li, 2002; Echevarria *et al.,* 2009), in oligotrophic waters the relative contribution of large cells is low but it quickly increases in more eutrophic environments. By exponential regression, the relation between the percentage of large cells of phytoplankton and total chlorophyll concentration is computed as $\%P_l = -17.92+69.87(1-e^{-3.705[Chla]})$. Thus, large phytoplankton concentration is found by applying $[P_l]=\%P_l x[Chla]/100$ and small phytoplankton $[P_s]=[P_t]-[P_l]$. In this way, the concentration of both phytoplankton types at the boundaries of the model is derived from satellite values (*i.e.* using the climatologic seasonal cycle of *[Chla]*), and applying the above mentioned relationships.

There is no meaningful information about zooplankton size distribution in the studied region but we can assume that the presence of large phytoplankton enhances the growth of large zooplankton and vice-versa. Thus, the same expressions were applied to both large and small zooplankton. Since no information was available about detritus, we used a constant value of 0.02 (mMol N m^{-3}) for small and large detritus (ROMS default value) for the initial fields and boundary values.

Boundary conditions were set using climatological monthly data in a 40 km wide restoring band along the boundaries. Initial and climatological boundary fields were prepared using ROMS tools package (Penven *et al.,* 2008).

Atmospheric forcing is taken from *Weather Research and Forecasting* (WRF version 3.1.1; Skamarock, 2008) as described and validated by Soares *et al.* (2012) and Cardoso *et al.* (2013). The simulation grid is centred in the Iberian Peninsula and covers the biogeochemical-ocean coupled model domain. The ocean model was forced by 4 h averaged outputs from WRF with 9 x 9 km resolution covering the period 1989 – 2008 (Soares *et al*., 2012).

Guadalquivir Estuary Parameterization

Our model is connected to a virtual estuary representing Guadalquivir River input to the marine shelf ecosystem. A source point was settled at 6.38°W longitude and 36.76°N latitude (Fig. 1), enabling the discharge of riverine-like waters. Monthly values of riverine water characteristics have been measured at La Señuela point within the Guadalquivir estuary by the Confederación Hidrográfica del Guadalquivir for several decades (1989 – 2009). This dataset was used to build a climatologic seasonal cycle of temperature and nitrate, whereas the other tracers in river waters were set to zero. Dam discharges from the same database were used as river run-off flows, and were kept daily to retain changes in nearby ecosystems due to specially rainy or dry years.

Since tides were not included, mixing along the shallow shelf areas is underrepresented. To overcome this limitation at the river point source, a tidal mixing parameterization was included in order to represent nutrient increase in the estuary owing to tidal mixing processes. Total river caudal Q_{Total} ($m^3 s^{-1}$) at river source point is equal to both river run-off $Q_{Run\text{-}off}$ plus tidal mixing Q_{Tide} contributions: $Q_{Tide} = Q_{Run\text{-}off} + Q_{Tide}$

Fick's law states that wherever a substance gradient exists, the substance will have the natural tendency to move in the medium in order to distribute itself. Applying it to the nitrate concentration gradient it becomes:

$$J = k_h \frac{\partial [NO_3]}{\partial y} \qquad (12)$$

where J is the mass diffusion flux (mol $m^{-2} s^{-1}$), k_h the horizontal diffusion coefficient of nitrate ($m^2 s^{-1}$) and $[NO_3]$ the concentration of nitrate (mol N m^{-3}) along the y-axis. The total nitrate flux I across a boundary ($mMols^{-1}$), i.e. the nitrate input rate at river source point due to tides is:

$$I_{Tide} = J \times A_{section} = -k_h \frac{\partial [NO_3]}{\partial y} \times A_{section} = k_h \frac{[NO_3]_{River}}{\mathrm{d}_{River}} \times A_{River}$$

The derivative of nitrate with respect to y can be approximated to the difference of nitrate concentration between the river and sea, and thus as river nitrate concentration $[NO_3]_{River}$ is much higher than in the sea we considered $[NO_3]_{Sea} \approx 0$. The scalar quantities d_{River} and A_{River}, are related to the river-sea diffusion interface.

Recalling that a river source point is a discharge point, nutrient input contribution by tidal mixing must be converted into a caudal-like term. Total nitrate flux is equal to the caudal multiplied by nitrate concentration of riverine waters and so our new Q_{Tide} term is given by:

$$I_{Tide} = Q_{Tide} \times [NO_3]_{River} \Leftrightarrow Q_{Tide} = k_h \frac{1}{d_{River}} \times A_{Tide} \qquad (14)$$

When entering the system, the Q_{Tide} term is multiplied by $[NO_3]_{River.}$ from Ruiz *et al*. (2015), we defined a rectangular vertical interface with A_{River} = 5800 m^2 and a distance of d_{River} = 3 km. The year cycle of the diffusion coefficient for nitrate at Guadalquivir was obtained from Diez-Minguito *et al*. (2012), using 2009 year data from Alcala Dam.

The year cycle of Q_{Tide} (not shown) is almost constant throughout the year, representing a continuous source of nitrate for our virtual estuary. Besides, according to our parameterization and assumptions, the contribution of this term is of the same order of magnitude as the mean river

run-off $Q_{Run\text{-}off}$, playing a comparable role in nutrient input.

In the river discharge region, the entry of riverine-like waters produces strong bio-tracer gradients together with strong velocity shear, producing an overshoot that destabilizes the advection-diffusion numerical scheme. This issue has been solved as in Peliz *et al*. (2013a) regarding strait overshooting problems. A Smagorinsky mixing coefficient is implemented to increase mixing and diffusion. This coefficient is maximum at 6.35°W longitude and 36.79°N latitude, next to the river source point, and decays radially within a 15 km zone. The decay is governed by a space sinus function. The entire water column is affected by the calculated Smagorinsky coefficient.

Satellite data

In order to evaluate model performance, sea surface temperature (SST) and surface chlorophyll (Chla) concentration were obtained from different satellite missions. SST was acquired from the 4 km Advanced Very High-Resolution Radiometer (AVHRR) Pathfinder Version 5 sea surface temperature (SST) dataset. AVHRR Oceans Pathfinder SST data were obtained from the Physical Oceanography Distributed Active Archive Center (PO.DAAC) at the NASA Jet Propulsion Laboratory, Pasadena, CA (http://podaac.jpl.nasa.gov). Weekly (8-days) SST images from 1989 to 2009 were used.

Ocean surface Chla data were downloaded from the GlobColour Project (http://www.globcolour.info/), which produces global ocean colour maps (Level-3) by merging the data from the three sensors SeaWiFS, MODIS and MERIS. Surface Chla data corresponds to product chlorophyll-a Case I water based on the GSM merging method (Maritorena & Siegel, 2005; Maritorena *et al.,* 2010). Weekly (8-days) surface Chla concentration images from 1998 to 2009 with ~4 km resolution were used.

Both satellite products were extracted for the area covered by our model domain (Fig. 1). Simulated sea surface temperature was extracted from the first sigma vertical level for comparison with satellite SST. Averaged simulated chlorophyll concentrations within the first 10 meters of the water column were used to compare with satellite-derived Chla measurements, as preliminary analysis of model results indicated that the first optical depth (i.e. where incident light reduces to 63%) is usually located close to this depth level. In order to obtain consistent data matrices, the simulated fields were interpolated onto the SST and Chla grid, respectively.

Zooplankton data

Zooplankton larger than 200 mm (i.e. mesozooplankton) collected during periodic cruises in the GoC shelf region, between the Guadiana River mouth and Trafalgar Cape, is used here to assess our model results. For the periods March 2002 - September 2004 and May 2005 - August 2007, monthly cruises were conducted on board the RV *Regina Maris* covering a grid of 30 stations (e.g. Prieto *et al*., 2009) from the coast to the continental shelf slope. The distance between the coastline and sampling stations ranged from 3 km to 35 km (average of 19 km) with depths varying from 15 m to 150 m (Prieto *et al*., 2009).

Mesozooplankton samples were collected at all stations following the same procedure. At each sampling point, double-oblique plankton hauls were conducted up to 100 meters (depth-permitting) using a Bongo net with a 40-cm mouth diameter and 200 mm mesh size. Henceforth, as sampling stations were located exclusively over the continental shelf, total integrated mesozooplankton biomass in those stations was effectively measured. All tows were performed at a vessel speed of 2-2.5 knots. Mesozooplankton concentration (ml m^{-3}) was quantified by estimations of sedimented plankton volumes and the integrated total zooplankton concentration (ml m^{-2}) was obtained by multiplying this value by the maximum sampled depth.

The averaged total integrated mesozooplankton concentration distribution was calculated from 2002 to 2007 on the shelf of the Gulf of Cadiz, and was then interpolated to our model regular grid using the *kriging* interpolation method.

Simulated large zooplankton concentration (in μM N kg^{-1}) was converted to the equivalent carbon weight (μg C kg^{-1}) assuming the Redfield C:N ratio (Redfield, 1934) and then into wet weight (μg kg^{-1}) using the logarithmic relation from Wiebe *et al.* (1975) and Wiebe (1988). Wet weight was converted into volume (ml m^{-3}) by assuming water density (ρ_w ~1 x 10^3 kg m^{-3}). Total integrated large zooplankton (ml m^{-2}) from our simulation was obtained considering zooplankton concentrations within the first 100 m (depth permitting) of the water column (approximately the maximum sampling depth). Simulated total integrated zooplankton was averaged for the same period and locations where cruises were performed.

Results

An extensive validation of the physical model is provided by Peliz *et al*. (2013a, b). In this work we will center on the biological variables (surface Chla and integrated zooplankton biomass).

Climatological surface patterns

Comparison of modelled and measured climatological values of SST and surface Chla concentration is shown in Figure 3. The climatological SST distribution (Fig. 3, left panel) is similar in both the model and satellite for the period 1989 - 2008 (Fig. 3A and 3B). The open sea regions of both sub-basins are typically warmer with mean

SST reaching up to 20°C while the coastal zones show lower temperatures especially in regions where mixing and upwelling are common processes (Strait of Gibraltar and southern coast of Portugal). Absolute differences between measured and modelled SST (Fig. 3C) are quite low (global absolute mean difference ~ 0.28°C) whereas there is some stronger disagreement (up to 1°C) in the central coast of the GoC (where models underestimate SST) and in the region typically occupied by the Atlantic Jet (AJ) in the Alboran sea (where models overestimate SST). The general comparison made in the Taylor diagram (magenta star in Fig. 3D) shows quite good agreement with a standard deviation almost identical in the model and data, with a correlation coefficient of 0.83. Mean SST distributions during individual months are also compared in the Taylor diagram of Figure 3D. All data points (red dots) are quite close to the mean value, indicating that the model is performing in a consistent manner throughout the year. The month of June is the one where the correlation between the model and satellite SST is lower but, still, R value is over 0.7.

The distribution of mean surface Chla concentration is also quite well reproduced by the model for the period 1998 - 2008 (Fig. 3, right column). Higher surface Chla concentration is measured and simulated in coastal regions of the GoC and Alboran Sea and the trace of the AJ around the Western Anticyclonic Gyre can be seen on both maps (Fig. 3E and 3F). The Taylor diagram clearly shows this concordance, with the standard deviation being quite similar in the model and data and a correlation coefficient of over 0.7 (Fig. 3H). Differences are low in general with a mean absolute difference of ~ 0.11 mg m^{-3} (Fig. 3G). However, quite large differences could be found along the eastern coast of the GoC where the model underestimates

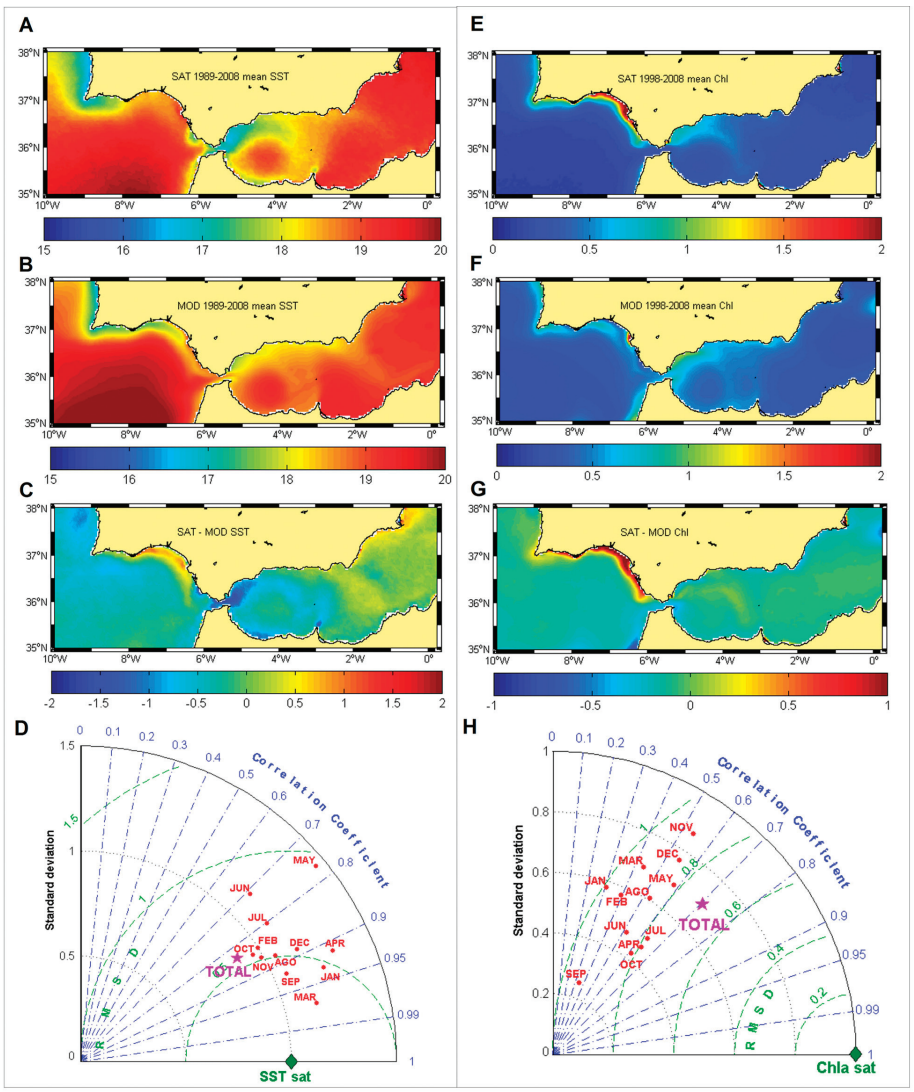

Fig. 3: Climatological horizontal distribution of observed and modelled SST (°C, left panel) and Chla (mg Chla m-3, right panel). Panels A and E show field data distributions. Panels B and F show the corresponding model simulations. Panels C and G correspond with the absolute differences between observed and modelled variables. Panels D and H show the Taylor diagrams for model-data comparison.

mean surface Chla by as much as 1 mg m^{-3}. Monthly climatologic Chla distributions are also quite reasonably reproduced by the model (Fig. 3H) with the majority of data points (red dots) showing R values between 0.45 and 0.67. September and January, however, seem to be less well represented by the model as the correlation coefficients are just 0.37 and 0.32, respectively.

Available zooplankton data is too scarce to allow a thorough comparison with model simulation. Instead, integrated mesozooplankton biomass within the shelf region of the GoC is compared with observations (Fig. 4). In both the model and observations, there is a clearly marked maximum situated over the continental shelf slope extending from North to South with a local maximum located in front of the Guadalquivir River (Fig. 4A and 4B). The time evolutions of measured and modelled mesozooplankton (Fig. 4C) are also quite similar, with a clear annual cycle (maximum level in winter-spring and minimum in late summer-autumn) and an increasing trend through the sampling period (2002 - 2007). Despite the coherence between observed and simulated mesozooplankton values (Fig. 4), the former shows a larger range of values compared to the latter. This prevents direct comparison of modelled and observed values and also explains the much lower standard deviation in simulated zooplankton shown in the Taylor diagram (Fig. 4D).

Seasonal Chla evolution

In order to assess the model's skill to reproduce seasonal productivity patterns, the studied domain has been divided into 7 different bio-regions with coherent dynamics on surface Chla seasonal patterns (Fig. 1). Regions 1 to 5 are located within the GoC and are based on the regionalization made by Navarro & Ruiz (2006), while regions 6 and 7 are located in the western Alboran Sea and are based on the analysis of Macias *et al*. (2007a). Climatologic seasonal patterns of surface Chla from the model and data in each of these regions are compared in Figure 5. The model seems to reproduce correctly the magnitude and timing of the seasonal Chla evolution in open-sea regions both on the Atlantic side (R1, Fig. 5A) and the Mediterranean side (R6, Fig. 5F) with correlation coefficients higher than 0.8 for both regions (Fig. 5H). Also, seasonal patterns in regions R3 and R4 located over the continental shelf of the GoC (Fig. 1) are quite well simulated in the model with correlation coefficients ~ 0.7 (Fig. 5H) and similar amplitude of the annual cycle (Fig. 5C and 5D). However, in both regions satellite-measured Chla is consistently higher than simulated values, as also shown above in the horizontal comparison in Figure 3 (right panel).

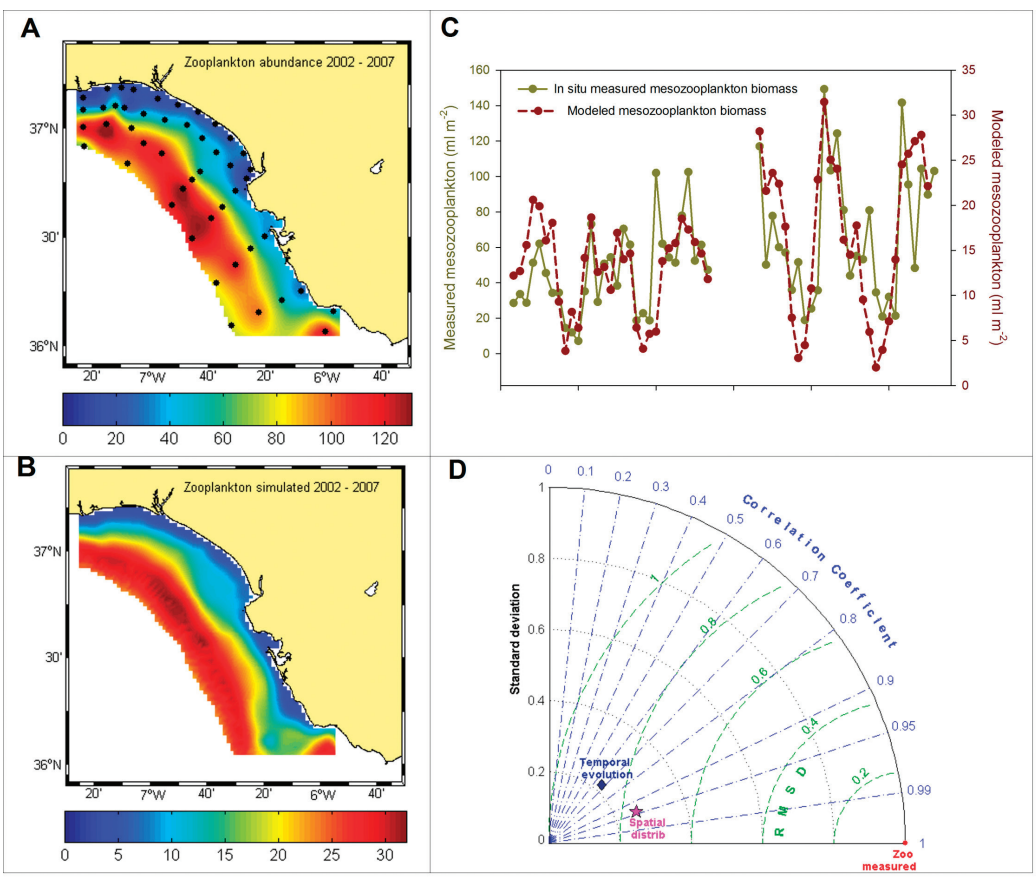

Fig. 4: Observed and modelled integrated (0 - 100 m) mesozooplankton biomass (ml m-2). A) Mean distribution from in-situ data, B) Mean distribution from model simulation, C) Time evolution of measured and simulated biomasses and D) Taylor diagram for model-data comparison.

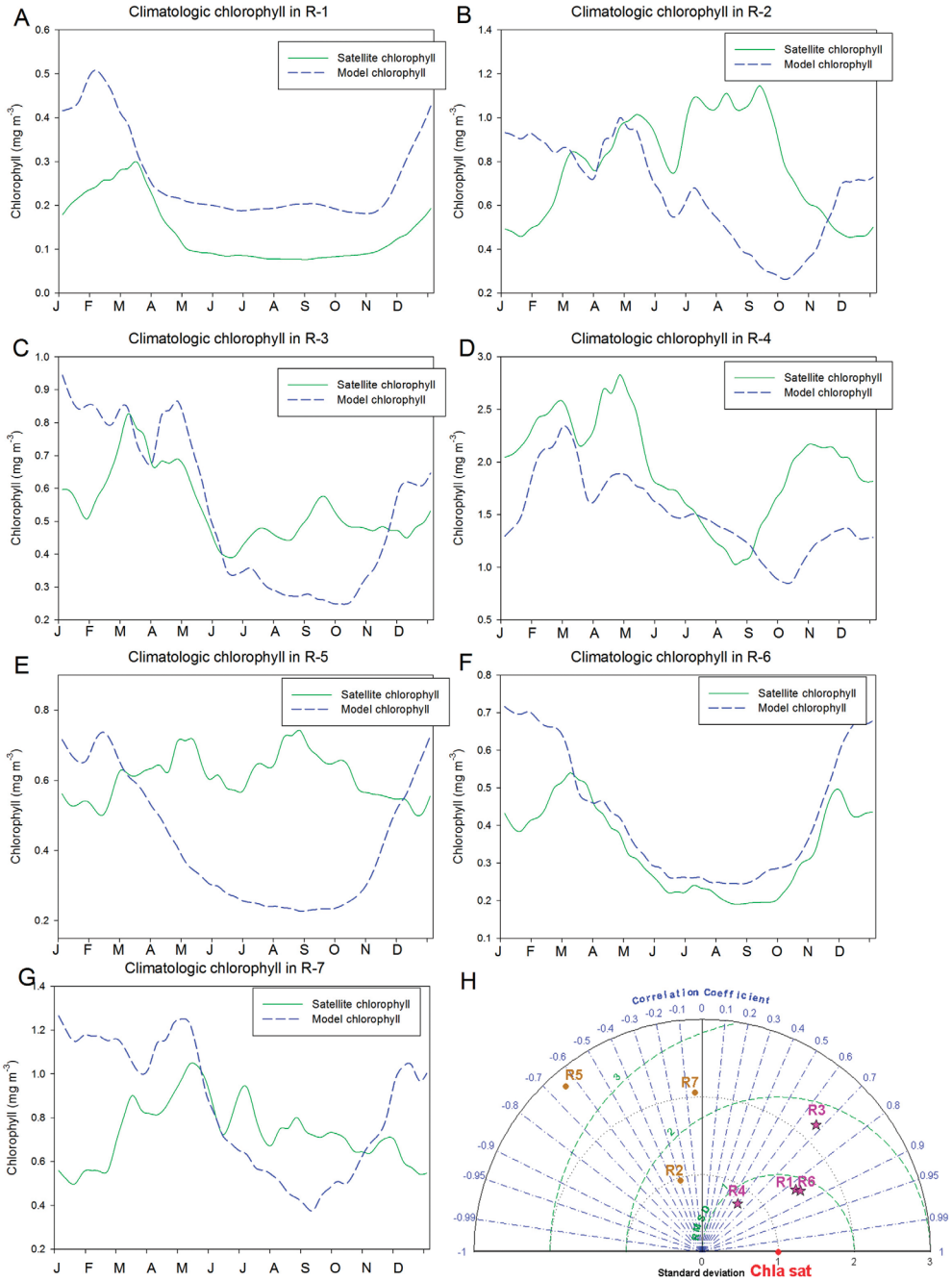

Fig. 5: Climatological seasonal cycles of measured (green lines) and modelled (blue line) surface chlorophyll concentration in the seven eco-regions shown in Fig. 1 (panels A to G). Taylor diagram of the seven comparisons (panel H). Statistically-significant ($p<0.05$) correlations are shown as magenta stars while non-significant correlations ($p>0.05$) are shown as brown circles.

Seasonal Chla evolutions in regions R2 (Cape S. Vincent area), R5 (Cape Trafalgar zone) and R7 (Estepona upwelling) are not well captured in the model (Fig. 5H). In all cases, correlation coefficients are negative, with modelled Chla reaching maximum values when measured levels are lowest (Fig. 5B, 5E and 5G).

Discussion

The proposed model is (to the best of our knowledge) the unique 3D hydrodynamic-biogeochemical simulation tool able to represent the main characteristics of the southern Iberia regional seas. The suitability of the model to simulate mean hydrodynamic conditions in the region has already been shown in Peliz *et al*. (2013a) and also its capability to simulate inter-basin water interchanges in hindcasting mode (Boutov *et al.,* 2014).

The biogeochemical model used here is quite similar to the one developed for different regions of the Mediterranean Sea by Oguz *et al.* (2013) on a 1D configuration and also to the one used by Macias *et al*. (2014) to simulate the 3D dynamics of the pelagic ecosystem of the open Mediterranean basin. Our

comparison of observed and simulated biological variables (Chla and mesozooplankton biomass) indicates that the proposed biogeochemical model is also suitable for representing the different ecosystems found in this particular region. Henceforth, this biogeochemical code could be considered as containing the minimum elements necessary to represent the main characteristics of pelagic ecosystems in a regional context.

However, the large discrepancy between observed and modelled mesozooplankton biomass values (Fig. 4) requires further investigation. First of all, it must be considered that modelled zooplankton is a closure term of the model and not an accurate representation of the real zooplankton compartment, a common problem to all low trophic level models (e.g. Fasham *et al*., 1990; Macias *et al*., 2012). Also, as pointed out by Lohman (1908), the sedimentation technique that produced mesozooplankton *in-situ* data can overestimate its abundance by a factor between 4 and 51. Thus, maximum measured total mesozooplankton bio-volume can actually be between 2.55 and 32.5 ml m^{-2}, falling within the range of mesozooplankton values obtained with the simulations. Therefore, mesozooplankton biomass comparisons should only be considered a qualitative exercise.

Concerning surface Chla, even if the performance of the model could be considered generally adequate (as shown by the Taylor diagram in Fig. 3H) there are some obvious problems and mismatches in certain areas that could have different origins. For example, in many coastal regions of the GoC the model underestimates the concentration of surface Chla (Fig. 3G) over the continental shelf. The seasonal evolution of Chla in those regions (regions R3 and R4 in Fig. 1) is quite well captured by the model (Fig. 5) although a quasi-permanent underestimation is simulated along the seasonal cycle (Figs. 5C and 5D). Here we must consider that only one river (the Guadalquivir) is contemplated in our model set-up while several other (smaller) rivers discharging in the zone are not included. This could lead to smaller simulated production because of lower riverine fertilization, although the Guadalquivir has been typically described by far as the main contributor to marine coastal productivity in the GoC (e.g. Prieto *et al*., 2009).

Also, the mismatch between observed and modelled Chla in this coastal region could be partially due to the well-known overestimation of satellite-derived estimates in type II coastal waters (e.g. Ruddick *et al*., 2000). In regions with high sediment loads and concentration of humic substances, algorithms to derive Chla concentration fitted for open sea regions tend to overestimate real Chla values (Toole & Siegel, 2001; Otero & Siegel, 2004). This is also true for the GoC where satellite estimates of Chla concentrations seems to fit very well with *in-situ* measures in the open sea regions (e.g. Navarro & Ruiz, 2006) while quite a consistent bias has been described for coastal, shallow regions (Caballero *et al*., 2014). Henceforth, the large differences between observed and modelled Chla values along the coast of the GoC could be due to a combination of an overestimation of satellite data and an underestimation of model simulation, the true value being somewhere in between.

In this GoC coastal area there is also a clear underestimation of modelled SST when compared with observations (Fig. 3C). This underestimation happens in a narrow band parallel to the coast along the continental shelf break (Fig. 3C). This is the region typically occupied by the 'Huelva front' (Garcia *et al.,* 2002) created by the upwelling of deep waters along the submarine canyon of Cape Santa Maria further west (Bruno *et al.,* 2006). The colder-than-observed surface waters in our model could be an indication that the upwelling process in this region is being overestimated by the hydrodynamic model. This should be studied in future model implementations.

It is worth mention here that the model setup did not include a benthic compartment that is not relevant in open-water settings but must be of importance in shallower regions near the coast. This is particularly important when considering the effect that suspended particles (mainly sediments and terrestrial runoffs) have on primary production around the Guadalquivir River mouth (e.g. Prieto *et al.,* 2009; Ruiz *et al.,* 2013). Very close to the estuary, the limiting factor for primary production is not nutrient availability (which is usually in excess) but light (e.g. Navarro *et al.,* 2012). This light limitation is mainly caused by extremely high levels of suspended sediments in this coastal region (e.g. Ruiz *et al.,* 2013; Caballero *et al.,* 2014). Not incorporating the effect of suspended material on the light environment of the model could be partially responsible for the larger differences between observed and modelled Chla levels in the coastal regions of the GoC.

Another evident short-cut in the physical model setup is the lack of tidal dynamics. Tides are of little importance in the Alboran Sea but they are relevant in GoC shallow areas and, specially, in the Strait of Gibraltar. Tidally-induced currents could be important in shallow, coastal regions where the continental shelf is wide (Sammari *et al.,* 2006) as is the case of the GoC (e.g. García-Lafuente *et al*., 2006). The effect of these tidally-induced currents would be to increase the sediment/water interchange and also to favour estuary/coastal mixing, thus enhancing nutrient loads in the marine environment.

A clear example of the importance of the tides is the Guadalquivir estuary. Preliminary simulations with our model were performed only considering river run-off from the estuary and neglecting tidal contribution (see Methods). In such runs (results not shown), only significant biological productivity was simulated at the river mouth during autumn and winter when precipitation is important, with the rest of the year showing very low production (in this simulation, mean annual phytoplankton biomass computed for R4 was 50% lower than its actual values). This is certainly not the annual cycle described for this region in previous works (e.g.

Navarro & Ruiz, 2006; Prieto *et al*., 2009) and not the one observed in the satellite record (Fig. 5D). With the inclusion of the tidal mixing parameterization explained above, simulated production levels increased to nearly the same range as observed values and the seasonal cycles were also more similar. However, the fact that climatological mean surface Chla is lower in the model than in the data for this particular region (Fig. 3G) could be indicating that we are still missing an important part of the coastal mixing processes induced by tidal dynamics.

As already commented, the importance of tides within the GoC is larger the closer we get to the Strait of Gibraltar. This is evident, for example, when examining R5 around Cape Trafalgar (Fig. 5E). In this case, the correlation coefficient is negative and quite high, indicating that the model is not able to even pick-up the right seasonality given that maximum simulated Chla levels are found during winter while observed maximum levels are reached during spring and at the end of summer. It has already been noted that surface Chla seasonality in this R5 is mostly related with the fortnightly and seasonal variations of tidal amplitude (Navarro & Ruiz, 2006; Navarro *et al.,* 2011); therefore, 'misbehaviour' of the model in this region is expected.

The same could be said for R7 with a negative insignificant correlation between the model and the data (Fig. 5H). Primary production dynamics in this region is linked to the coastal upwelling which is favoured by wind forcing (e.g. Sarhan *et al*., 2000; Macias *et al*., 2009) and by the dynamics of the Atlantic jet (AJ) entering through the Strait of Gibraltar (e.g. Macias *et al*., 2007b). Both mechanisms are linked (at the subinertial scale) through the effects that sea level pressure over the western Mediterranean has on AJ velocity (e.g. Candela *et al*., 1989) and on local wind conditions (Macias *et al*., 2007a). However, the AJ dynamics are also strongly influenced by the tidal baroclinic forcing at the Strait (e.g. Sanchez-Garrido *et al*., 2013), which is missed in our model. Tidal mixing within the main channel of the Strait fertilizes the AJ (e.g. Macias *et al.,* 2006; Ramírez-Romero *et al.,* 2014) enhancing primary production on the western shelf of the Alboran Sea (Macias *et al.,* 2007a) and explaining the higher observed Chla concentration with respect to the model simulations.The missing tidal effect is also visible in the simulated SST, as this region is too warm when compared with observations (Fig. 3C). Periodic enhancement of AJ velocity in the main channel of the strait favours interfacial mixing (e.g. Bruno *et al*., 2002; García-Lafuente *et al*., 2002) and could be easily identified by remote sensing as a strong cooling of surface waters (e.g. Bruno *et al.,* 2013). Our model, even if correctly reproducing the mean fluxes through the Strait (Peliz *et al*., 2013b), is lacking these cyclic, recurrent mixing processes and, hence, simulates warmer than observed SST.

Finally, the mismatch between observed and simulated Chla in R2 around Cape San Vincent (Fig. 5H) could, very likely, be related with the geographical position of this zone in close vicinity with the model boundaries (Fig. 1). This area around Cape San Vincent presents productivity dynamics clearly linked with the upwelling region off the western Portuguese coast (Navarro & Ruiz, 2006). Observed Chla presents maximum values during summer (Fig. 5B), coincident with maximum intensity northerly winds along the Portuguese coast, which favours upwelling (Fiúza, 1983; Relvas & Barton, 2002) in this eastern boundary current system (García-Lafuente & Ruiz, 2007). Our model, however, simulates maximum concentrations during winter-spring and does not capture the observed seasonality.

Despite the limitations indicated above, the proposed model could be a useful tool for gaining a comprehensive understanding of the functioning of the southern Iberia regional seas. The additional computational effort necessary to run the ocean model with this ecosystem model is not disproportionate when compared with the model containing only physical processes. Therefore, using a double compartment model is a good compromise to resolve lower trophic levels in the Gulf of Cadiz and the Alboran Sea without adding an excessive numerical burden.

With the appropriate atmospheric forcing and boundary conditions, this tool will help to understand the past (hindcast) and future (forecast) evolution of the region. Still, some work is needed in order to reduce the current mismatch between observations and simulations, especially regarding the effect of tidal dynamics and the inclusion of some additional fertilization sources (mainly rivers) in the model configuration. This refinement would bring greater accuracy to simulated biogeochemical fields on the shelf of the Gulf of Cadiz and the western Alboran Sea.

Acknowledgements

This work was supported by E.U. projects MarinERA-MedEX (CTM2008-04036-E/MAR) and PERSEUS (Ref. 287600) as well as by the Spanish National Research Projects FCT MARIN-ERA/MAR/0002/2008 and CTM2011-22580. DM was supported by a Grantholder Cat.30 position of the Joint Research Center of the European Commission. LP was supported by a grant from the Ramon y Cajal Programme, from the Spanish MINECO.

References

Armi, L., Farmer, D., 1985. The internal hydraulics of the Strait of Gibraltar and associated sill and narrows. *Oceanologica Acta,* 8, 37-46.

Baldó, F., García-Isarch, E., Jiménez, M.P., Romero, Z., Sánchez-Lamadrid, A. *et al*., 2006. Spatial and temporal distribution of the early life stages of three commercial fish species in the northeastern shelf of the Gulf of Cádiz. *Deep-Sea Research II*, 53, 1391-1401.

Boutov, D., Peliz, A., Miranda, P.M.A., Soares, P.M.M., Cardoso, R.M. *et al*., 2014. Inter-annual variability and

long term predictability of exchanges through the Strait of Gibraltar. *Global and Planetary Change*, 114, 23-37.

Bruno, M., Alonso, J.J., Cózar, A., Vidal, J., Ruiz-Cañavate, A. *et al*., 2002. The boiling-water phenomena at Camarinal Sill, the strait of Gibraltar. *Deep-Sea Research II,* 49, 4097-4113.

Bruno, M., Chioua, J., Romero, J., Vázquez, A., Macías, D. *et al*., 2013. The importance of sub-mesoscale processes for the exchange of properties through the Strait of Gibraltar. *Progress in Oceanography*, 116, 66-79.

Bruno, M., Vazquez, A., Gomez-Enri, J., Vargas, J.M., Garcia-Lafuente, J. *et al*., 2006. Observations of internal waves and associated mixing phenomena in the Portimao Canyon area. *Deep Sea Research II*, 53 (11-13), 1219-1240.

Caballero, I., Morris, E.P., Prieto, L., Navarro, G., 2014. The influence of the Guadalquivir River on spatio-temporal variability of suspended solid and chlorophyll in the eastern Gulf of Cadiz. *Mediterranean Marine Science*, 15 (4), 721-738..

Candela, J., Winant, C., Bryden, H., 1989. Meteorologically forced subinertial flows through the Strait of Gibraltar. *Journal of Geophysical Research*, 94, 12667-12679.

Catalán, I., Jiménez, M.T., Alconchel, J.I., Prieto, L., Muñoz, J.L., 2006. Spatial and temporal changes of coastal demersal assemblages in the Gulf of Cadiz (SW Spain) in relation to environmental conditions. *Deep-Sea Research II*, 53, 1402-1419.

Cardoso, R.M., Soares, P.M.M., Miranda, P.M.A., Belo-Pereira, M., 2013. WRF high resolution simulation of Iberian mean and extreme precipitation climate. *International Journal of Climatology*, 33, 2591-2608.

Colella, P., Woodward, P.R., 1984. The Piecewise Parabolic Method (PPM) for Gas-Dynamical Simulations. *Journal of Computational Physics*, 54. 178-201.

Diez-Minguito, M., Baquerizo, A., Ortega-Sánchez, M., Navarro, G., Losada, M.A., 2012. Tide transformation in the Guadalquivir estuary (SW Spain) and process-based zonation. *Journal of Geophysical Research*, 117, C03019.

Echevarria, F., Zabala, L., Corzo, A., Navarro, G., Prieto, L. *et al*., 2009. Spatial distribution of autotrophic picoplankton in relation to physical forcings: the Gulf of Cádiz, Strait of Gibraltar and Alborán Sea case study. *Journal of Plankton Research,* 33, 1339-1351.

Eppley, R.W., 1972. Temperature and phytoplankton growth in the sea. *Fisheries Bulletin*, 70, 1063-1085.

Fasham, M.J.R., Ducklow, H.W., McKelvie, S.M., 1990. A nitrogen-based model of plankton dynamics in the oceanic mixed layer. *Journal of Marine Research,* 48, 591-639.

Fiúza, A.F.G., 1983. Upwelling patterns off Portugal. p. 85-98. In: *Coastal Upwelling: Its Sediment Records, Part A*. Suess, E., Thiede J. (Eds). Plenum, New York.

Garcia, C.M., Prieto, L., Vargas, M., Echevarria, F., Garcia-Lafuente, J. *et al*., 2002. Hydrodynamics and the spatial distribution of plankton and TEP in the Gulf of Cadiz (SW Iberian Peninsula). *Journal of Plankton Research*, 24, 817-833.

García-Lafuente, J., Ruiz, J., 2007. The Gulf of Cádiz pelagic ecosystem. *Progress in Oceanography*, 74, 228-251.

García-Lafuente, J., Delgado, J., Criado-Aldeanueva, F., Bruno, M., del Río, J. *et al*., 2006. Water mass circulation on the continental shelf of the Gulf of Cádiz. *Deep-Sea Research II,* 53, 1183-1197.

García-Lafuente, J., Delgado, J., Vargas, J.M., Vargas, M., Plaza, F. *et al*., 2002. Low frequency variability of the exchanged flows through the Strait of Gibraltar during CANIGO. *Deep-Sea Research II,* 49, 4051-4067.

Huete-Ortega, M., Calvo-Díaz, A., Graña, R., Mouriño-Carballido, B., Marañón, E., 2011. Effect of environmental forcing on the biomass, production and growth rate of size-fractionated phytoplankton in the central Atlantic Ocean. *Journal of Marine Systems*, 88, 203-213.

Koné, V., Machu, E., Penven, P., Andersen, V., Garçon, V. *et al*., 2005. Modeling the primary and secondary productions of the southern Benguela upwelling system: A comparative study through two biogeochemical models. *Global Biochemical Cycles,* 19, GB4021.

Li, W.K.W., 2002. Macroecological patterns of phytoplankton in the northwestern North Atlantic Ocean. *Nature,* 419, 154-157.

Lohman, H., 1908. Uber die bezichungen zwischen den pelagischen ablagerungen und dem plankton des meres. *International Revve der Gasamten Hydrobiologie und Hydrographie*, 1, 303-323.

Macias, D., Bruno, M., Echevarría, F., Vázquez, A., García, C.M., 2008a. Metereologically-induced mesoscale variability of the North-western Alboran Sea (southern Spain) and related biological patterns. *Estuarine, Coastal and Shelf Science,* 78, 250-266.

Macias, D., Franks, P.J.S, Ohman, M.D., Landry, M.R., 2012. Modelling the effects of coastal wind- and wind-stress curl-driven upwellings on plankton dynamics in the Southern California Current system. *Journal of Marine Systems,* 94, 107-119.

Macías, D., García, C.M., Echevarría, F., Vázquez-Escobar, A., Bruno, M., 2006. Tidal induced variability of mixing processes on Camarinal Sill (Strait of Gibraltar).A pulsating event. *Journal of Marine Systems,* 60, 177-192.

Macias, D., Lubian, L.M., Echevarría, F., Huertas, E., García, C.M., 2008b. Chlorophyll maxima and water mass interfaces: tidally induced dynamics in the Strait of Gibraltar. *Deep-Sea Research I,* 55, 832-846.

Macias, D., Martin, A.P., García-Lafuente, J., García, C.M., Yool, A. *et al*., 2007b. Mixing and biogeochemical effects induced by tides on the Atlantic-Mediterranean flow in the Strait of Gibraltar. An analysis through a physical-biological coupled model. *Progress in Oceanography,* 74, 252-272.

Macias, D., Navarro, G., Bartual, A., Echevarría, F., Huertas, I.E., 2009. Primary production in the Strait of Gibraltar: carbon fixation rates in relation to hydrodynamic and phytoplankton dynamics. *Estuarine Coastal and Shelf Science,* 83, 197-210.

Macias, D., Navarro, G., Echevarría, F., García, C.M., Cueto, J.L., 2007a. Phytoplankton pigment distribution in the north-western Alboran Sea and meteorological forcing: a remote sensing study. *Journal of Marine Research*, 65, 523-543.

Macias, D., Stips, A., Garcia-Gorriz, E., 2014. The relevance of deep chlorophyll maximum in the open Mediterranean Sea evaluated through 3D hydrodynamic-biogeochemical coupled simulations. *Ecological Modelling*, 281, 26-37.

Maritorena, S., Siegel, D.A., 2005. Consistent merging of satellite ocean color data sets using a bio-optical model. *Remote Sensing of Environment*, 94, 429-440.

Maritorena S., Hembise Fanton d'Andon, O., Mangin, A., Siegel, D.A., 2010. Merged satellite ocean color data products using a bio-optical model: characteristics, benefits and issues. Remote Sensing of Environment, 114 (8), 1791-1804.

Navarro, G., Ruiz, J., 2006. Spatial and temporal variability of phytoplankton in the Gulf of Cádiz through remote sensing

images. Deep-Sea Research II, 53 (11-13), 1241-1260.
Navarro, G., Caballero, I., Prieto, L., Vázquez, A., Flecha, S. *et al*., 2012. Seasonal-to-interannual variability of chlorophyll-a bloom timing associated with physical forcing in the Gulf of Cadiz. *Advances in Space Research*, 50 (8), 1164-1172.
Navarro, G., Ruiz, J., Huertas, I.E., García, C.M., Criado-Aldeanueva, F. *et al*., 2006. Basin scale structures governing the position of the subsurface chlorophyll maximum in the gulf of Cádiz. *Deep-Sea Research II,* 53, 1261-1281.
Navarro, G., Vázquez, A., Macías, D., Bruno, M., Ruiz, J., 2011. Understanding the patterns of biological response to physical forcing in the Alborán Sea (Western Mediterranean). *Geophysical Research Letters,* 38, L23606, doi:10.1029/2011GL049708.
Oguz, T., Macias, D., Renault, L., Ruiz, J., Tintore, J., 2013. Controls of plankton production by pelagic fish predation and resource availability in the Alboran and Balearic Seas. *Progress in Oceanography,* 112-113, 1-14.
Otero, M.P., Siegel, D., 2004. Spatial and temporal characteristics of sediment plumes and phytoplankton blooms in the Santa Barbara Channel. *Deep Sea Research II,* 51 (10), 1129-1149.
Parker, R.A., 1993. Dynamic models for ammonium inhibition of nitrate uptake by phytoplankton. *Ecological Modelling*, 66, 113-120.
Peliz, A., Boutov, D., Cardoso, R., Delgado, J., Soares, P., 2013a. The Gulf of Cadiz-Alboran Sea sub-basin: Model setup, exchange and seasonal variability, *Ocean Modelling*, 61, 49-67.
Peliz, A., Boutov, D., Teles-Machado, A. 2013b. The Alboran Sea mesoscale in a long term high resolution simulation: Statistical analysis, *Ocean Modelling*, 72, 32-52.
Penven P., Marchesiello, P., Debreu, L., Lefevre, J. , 2008. Software tools for pre- and post-processing of oceanic regional simulations. *Environmental Modelling Softw*are, 23, 660-662.
Prieto, L., Navarro, G., Rodríguez-Galvez, S., Huertas, I.E., Naranjo, J.M. *et al*., 2009. Oceanographic and meteorological forcing of the pelagic ecosystem on the Gulf of Cadiz shelf (SW Iberian Peninsula). *Continental Shelf Research,* 29, 2122-2137.
Ramírez-Romero, E., Macías, D., García, C.M., Bruno, M., 2014. Biogeochemical patterns in the Atlantic inflow through the Strait of Gibraltar. *Deep-Sea Research I*, 85, 88-100.
Redfield, A.C., 1934. On the proportions of organic derivatives in sea water and their relation to the composition of plankton. p. 177-192. In: *James Johnstone Memorial Volume*. Daniel, R.J. (Ed). University Press of Liverpool, Liverpool.
Relvas, P., Barton E.D., 2002. Mesoscale patterns in the Cape São Vicente (Iberian Peninsula) upwelling region. *Journal of Geophysical Research*, 107(C10), 3164.
Rubín, J.P., Cano, N., Rodríguez, V., Blanco, J.M., Jiménez-Gómez, F. *et al*., 1997. Relaciones del ictioplancton con la hidrología, biomasa fitoplanctónica, oxígeno disuelto y nutrientes, en el mar de Alborán y estrecho de Gibraltar (julio de 1993). *Publicacion Especializada Instituto Español de Oceanografia,* 24, 75-84.
Ruddick, K.G., Ovidio, F., Rijkeboer, M., 2000. Atmospheric correction of SeaWiFS imagery for turbid coastal and inland waters. *Applied optics*, 39 (6), 897-912.
Ruiz, J., Echevarría, F., Font, J., Ruiz, S., García, E. *et al*., 2001. Surface distribution of chlorophyll, particles and gelbstoff in the Atlantic jet of the Alborán Sea: from submesoscale to subinertial scales of variability. *Journal of Marine Systems,* 29, 277-292.
Ruiz, J., Gonzalez-Quirós, R., Prieto, L., Navarro, G., 2009. A Bayesian model for anchovy (*Engraulis encrasicolus*): the combined forcing of man and environment. *Fisheries Oceanography,* 18, 62-76.
Ruiz, J., Macías, D., Losada, M.A., Díez-Minguito, M., Prieto, L., 2013. A simple biogeochemical model for estuaries with high sediment loads: Application to the Guadalquivir River (SW Iberia). *Ecological Modelling,* 265,194-206.
Ruiz, J., Polo, M.J., Díez-Minguito, M., Navarro, G., Morris, E.P. *et al*., 2015. The Guadalquivir estuary: a hot spot for environmental and human conflicts. Chapter 8. p. 199-232. In: *Environmental Management and Governance. Advances in Coastal and Marine Resources*. Finkl, C.W., Makowski, C. (Eds). Springer, London.
Sammari, C., Koutitonsky, V.G., Mouss, M., 2006. Sea level variability and tidal resonance in the Gulf of Gabes, Tunisia. *Continental Shelf Research,* 26, 338-350.
Sanchez-Garrido, J.C., Garcia-Lafuente, J., Alvarez-Fanjul, E., Garcia-Sotillo, M., de los Santos, F.J., 2013. What does cause the collapse of the Western Alboran Gyre? Results from an operational ocean model. *Progress in Oceanography*, 116, 142-153.
Sarhan, T., García-Lafuente, J., Vargas, M., Vargas, J.M., Plaza, F., 2000. Upwelling mechanisms in the northwestern Alboran Sea. *Journal of Marine Systems,* 23, 317-331.
Shchepetkin, A.F., McWilliams, J.C., 2005. The regional ocean modeling system: a split-explicit, free-surface, topography following coordinates ocean model. *Ocean Modelling*, 9, 347-404.
Skamarock, W.C., 2008. A linear analysis of the NCAR CCSM finite-volume dynamical core. *Monthly Weather Review*, 136, 2112 – 2119.
Soares, P., Cardoso, R., de Medeiros, J., Miranda, P., Belo-Pereira, M. *et al*., 2012. WRF high resolution dynamical downscaling of ERA-Interim for Portugal. *Climate Dynamics*, 39, 2497-2522.
Toole, D.A., Siegel, D.A., 2001. Modes and mechanisms of ocean color variability in the Santa Barbara Channel. *Journal of Geophysical Research: Oceans (1978–2012),* 106 (C11), 26985-27000.
Vázquez, A., Flecha, S., Bruno, M., Macías, D., Navarro, G., 2009. Internal waves and short-scale distribution patterns of chlorophyll in the Strait of Gibraltar and Alborán Sea. *Geophysical Research Letters,* 36, L23601.
Wiebe, P.H. 1988. Functional regression equations for zooplankton displacement volume, wet weight, dry weight, and carbon: a correction. *Fisheries Bulletin*, 86, 833-835.
Wiebe, P.H., Boyd, S.H., Cox, J.L., 1975. Relationships between zooplankton displacement volume, wet weight, dry weight, and carbon. *Fisheries Bulletin*, 73, 777-786.